PHOTONICS Research

Measuring high orbital angular momentum of vortex beams with an improved multipoint interferometer

Qi Zhao,[1,2] Miao Dong,[1] Yihua Bai,[1] and Yuanjie Yang[1,*]

[1]School of Physics, University of Electronic Science and Technology of China, Chengdu 610054, China
[2]Southwest Institute of Technical Physics, Chengdu 610041, China
*Corresponding author: dr.yang2003@uestc.edu.cn

Received 3 December 2019; revised 7 March 2020; accepted 16 March 2020; posted 20 March 2020 (Doc. ID 384925); published 30 April 2020

A multipoint interferometer (MI), uniformly distributed point-like pinholes in a circle, was proposed to measure the orbital angular momentum (OAM) of vortex beams [Phys. Rev. Lett. 101, 100801 (2008)], which can be used for measuring OAM of light from astronomical sources. This is a simple and robust method; however, it is noted that this method is only available for low topological charge because the diffracted intensity patterns for vortex beams with higher OAM will repeat periodically. Here, we propose an improved multipoint interferometer (IMI) for measuring the OAM of an optical vortex with high topological charge. The structure of our IMI is almost the same as the MI, but the size of each pinhole is larger than a point in the MI. Such a small change enables each pinhole to get more phase information from the incident beams; accordingly, the IMI can distinguish any vortex beams with different OAM. We demonstrate its viability both theoretically and experimentally.

https://doi.org/10.1364/PRJ.384925

1. INTRODUCTION

Optical vortices with azimuthal phase $\exp(il\varphi)$ carry orbital angular momentum (OAM) of $l\hbar$ per photon, where l is the topological charge, $\hbar$ is the reduced Planck's constant, and φ is the azimuthal angle [1–3]. Vortex beams with OAM have found applications in many fields, such as quantum information processing [4,5], free-space communications [6,7], super-resolution microscopy [8], optical micromanipulations [9,10], and astronomical sources detection [11]. Accordingly, it is important to measure the topological charge (or OAM) of a vortex beam in many applications [11–16]. Until now, numerous methods have been developed for measuring the topological charge of vortex beams. For instance, we can use a spatial light modulator and monofiber to convert vortex beams to Gaussian beams by holographic techniques, while the efficiency is low [17]. The widely used method is to observe the interference pattern by interfering the wavefront of the vortex beam with its own mirror image or a reference wavefront, such as the Mach–Zehnder interferometer [18] and double-slit interference [19]. In 2008, Berkhout and Beijersbergen [20] presented a multipoint interferometer (MI) to detect the OAM of vortex beams by observing the interference patterns. It is shown that this method can find applications in measuring the OAM of light from astronomical sources. Later, a ring-sampled multipoint plate was developed for measuring the OAM of vortex beams based on the retrieving algorithm [21]. Also, we can measure the OAM by optical transformation, namely, converting the vortex beam with the spiral phase into a beam with a transverse phase gradient [22]. Besides the symmetrical structures, some asymmetric structures were also developed for measuring OAM, such as a screen with two nonparallel air slits [23], dynamic angular double slits [24], and a gradually changing period diffraction element [25]. More recently, several new devices, such as a translated single slit [26], single stationary lens [27], and gray-scale algorithm [28], have been introduced to determine the OAM of vortex beams. Furthermore, some methods for measuring fractional topological charge of vortex beams have been proposed as well [29–31]. Among the aforementioned methods, the multipoint interferometer (MI) is one of the most robust and simple. We found that such a simple MI can also be used to manipulate the OAM spectrum [32]. However, it is shown that the interference patterns, generated from the MI, will repeat periodically once the value of topological charge becomes larger than half-value of the number of pinholes. In other words, this method is only available for vortex beams with low topological charge [33].

In this work, we propose an improved multipoint interferometer (IMI), which is formed by uniformly distributed circular apertures instead of point-like pinholes, where the radius of aperture (r_0) is not negligible, as shown in Fig. 1, to solve such problems. The results demonstrate that the far-field interference patterns using such a method will not repeat any more for vortex beams with any topological charge. Therefore, the

IMI can be used to measure the vortex beams with high topological charge.

2. THEORY AND METHODS

A. Theory of IMI

The schematic for measuring the topological charge of an optical vortex by an IMI is illustrated in Fig. 1. When a vortex beam illuminates on the IMI, we can measure its OAM by detecting the interference patterns in the far field.

We start with the proposed method theoretically. The complex amplitude of the optical vortex beam in the source plane, namely, just after passing through the IMI, can be written as

$$o(x,y)=\sum_{n=1}^{N}\mathrm{circ}\left[\sqrt{(x-x_n)^2+(y-y_n)^2}/r_0\right]A_p^l, \quad (1)$$

where $\mathrm{circ}(x,y)$ is the transmittance function of the aperture, and x_n, y_n are the central coordinates of the nth aperture. The complex amplitude of Laguerre–Gaussian (LG) beams with topological charge l is given by

$$A_p^l(r,\phi)\propto r^l L_p^l\left(\frac{2r^2}{w^2}\right)\exp\left(-\frac{r^2}{w^2}\right)\exp(-il\phi), \quad (2)$$

where w is the waist size of the beam, $L_p^l(\cdot)$ is the associated Laguerre polynomial, and p and l are the radial and azimuthal mode index, respectively.

Considering the Fraunhofer limit, the intensity pattern I_p^l in the detector plane can be written as

$$\begin{aligned}I_p^l&\propto|\mathrm{FT}\{o(x,y)\}|^2\\&=\left|\sum_{n=0}^{N-1}\mathrm{FT}\{A_p^l(r,\phi,z)\}\otimes\left\{\frac{r_0J_1\left(2\pi r_0\sqrt{f_x^2+f_y^2}\right)}{\sqrt{f_x^2+f_y^2}}\right.\right.\\&\left.\left.\times\exp\left[-i\frac{ka}{f}(x\cos a_n+y\sin a_n)\right]\right\}\right|^2, \quad (3)\end{aligned}$$

where $\mathrm{FT}\{\cdot\}$ denotes the Fourier transform operator, and $\otimes$ is the convolution operator. J_1 is the Bessel function of the first order, f_x and f_y are given by $f_x=\frac{x}{\lambda z}$ and $f_y=\frac{y}{\lambda z}$, and $a_n=2\pi n/N$ is the azimuthal coordinate of the nth aperture.

Provided the radius of each aperture r_0 is small enough and can be neglected, the far-field intensity pattern can be reduced as [20]

$$I_p^l\propto\left|\sum_{n=0}^{N-1}\exp(-ila_n)\exp\left[-i\frac{ka}{f}(x\cos a_n+y\sin a_n)\right]\right|^2. \quad (4)$$

To demonstrate the power of our method, the simulated intensity patterns of vortex beams with different OAM diffracted by IMI with six circular apertures are shown in Fig. 2(a).

As a comparison, the corresponding results for MI are shown in Fig. 2(b) as well. From Fig. 2(a), we can see that, for IMI, all the intensity patterns differ significantly, even when the topological charge is larger than the number of apertures. Therefore, the OAM of the vortex beams can be measured by detecting the interference patterns directly. In Fig. 2(b), the intensity patterns repeat periodically from $l=4$, viz., the patterns are the same for $l=\{0,6\},\{1,5,7\},\{2,4,8\}\ldots$ The intensity patterns can be inferred to repeat periodically when the topological charges satisfy the equation $l_1-l_2=Nm$, or $l_1+l_2=Nm$, where $m=1,2,3,\ldots$, is an arbitrary integer, and N is the number of the pinholes in MI. For example, using MI, the interference pattern of the vortex beam with $l=1$ is the same as those with $l=5$ and $l=7$. Figure 1 shows that the MI with six pinholes does not work for vortex beams with $l>3$, while the IMI can still work for vortex beams with high topological charge.

B. Physical Explanation

Now, let's discuss why the intensity patterns can repeat for different topological charges using MI. Suppose we use two vortex beams to illuminate the MI successively, satisfying $l_1-l_2=Nm$. Then, the far-field complex amplitude of the beam passing through the nth pinhole can be written as

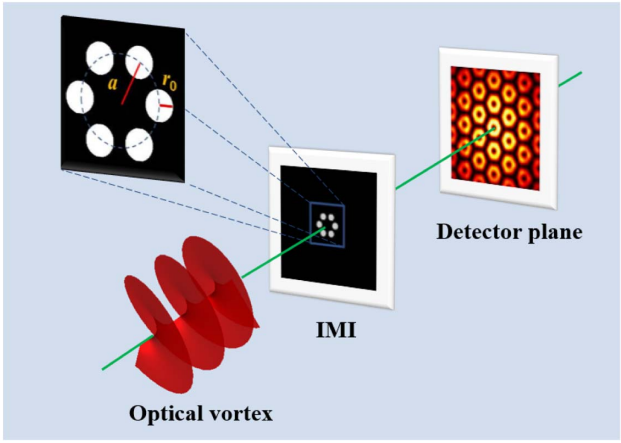

Fig. 1. Schematic of the experimental setup for detecting the topological charge of optical vortex with an IMI.

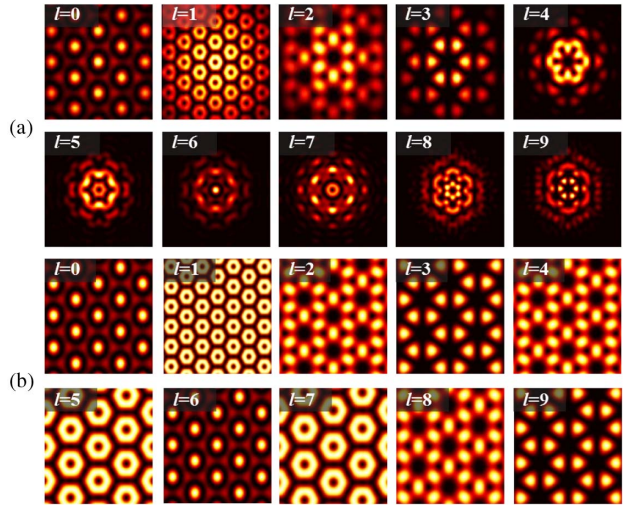

Fig. 2. Far-field intensity patterns for vortex beams with different topological charges diffracted by (a) IMI and (b) MI with $N=6$. (a) and (b) are calculated by Eqs. (3) and (4), respectively.

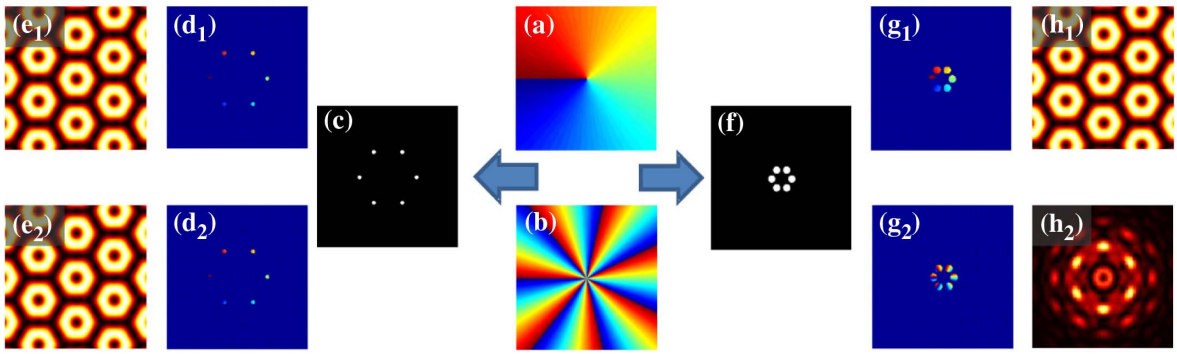

Fig. 3. Distinctions between the two methods with (c) MI and (f) IMI. (a) and (b) The phase distributions of vortex beams with $l = 1$ and $l = 7$, respectively. (d_1) and (d_2) are the corresponding local phase distributions obtained by MI for $l = 1$ and $l = 7$, respectively. (e_1) and (e_2) are the corresponding far-field intensity patterns, respectively. (g_1), (g_2), (h_1), and (h_2) are the same as (d_1), (d_2), (e_1), and (e_2) but for IMI.

$$E_n^{l_1} = \exp(-il_1a_n)\exp\left[-i\frac{ka}{f}(x\cos a_n + y\sin a_n)\right]$$
$$= \exp[-i(l_2 + Nm)a_n]\exp\left[-i\frac{ka}{f}(x\cos a_n + y\sin a_n)\right]$$
$$= \exp(-il_2a_n)\exp(-i2mn\pi)\exp\left[-i\frac{ka}{f}(x\cos a_n + y\sin a_n)\right]$$
$$= E_n^{l_2}. \quad (5)$$

This is why the intensity patterns for l_1 and l_2 are the same using the MI. For $l_1 + l_2 = Nm$, the situation is similar, and the expression for the far-field complex amplitude can be written as

$$E_n^{l_1} = \exp(-il_1a_n)\exp\left[-i\frac{ka}{f}(x\cos a_n + y\sin a_n)\right]$$
$$= \exp[-i(Nm - l_2)a_n]\exp\left[-i\frac{ka}{f}(x\cos a_n + y\sin a_n)\right]$$
$$= \exp[-i(-l_2)a_n]\exp(-i2mn\pi)$$
$$\times\exp\left[-i\frac{ka}{f}(x\cos a_n + y\sin a_n)\right]$$
$$= E_n^{l_2*}. \quad (6)$$

Here, * denotes the complex conjugate. Equation (6) shows that, if one uses MI, the interference patterns for l_1 and l_2 are the same when $l_1 + l_2 = Nm$.

To illustrate the new insight gained from our improved method, we visually analyze the two different interfering processes diffracted by MI and IMI, using the local phase information for vortex beams with $l = 1$ and 7 in Fig. 3. Figures 3(d_1) and 3(d_2) show that the local phase information obtained by MI is nearly the same, due to the tiny size of the pinhole, and consequently causes the identical interference patterns in Figs. 3(e_1) and 3(e_2). However, the local phase information obtained by the apertures in IMI [Fig. 3(g_2)] is obviously different from that in MI [Fig. 3(g_1)], due to the bigger size of the aperture and because the apertures are closer to the center of the beam axis, where the phase changes quicker than in the outer region. Accordingly, the distinguishable interference patterns can be observed [see Figs. 3(h_1) and 3(h_2)]. It is clear from Fig. 3 that, although the structure of our IMI is similar to MI, the IMI can get more phase information and can distinguish any vortex beams with different OAM.

3. EXPERIMENTAL RESULTS

To prove the feasibility of our proposed method, we measure the interference patterns diffracted by IMI experimentally. The experimental setup used to generate and measure the OAM of optical vortices is shown in Fig. 4. The measured vortex beams possessing OAM are generated by the spiral phase plate [34,35] displayed on a phase-only liquid crystal spatial light modulator (SLM_1, Holoeye PLUTO VIS), illuminated by a helium-neon laser with the wavelength of 632.8 nm that emits a Gaussian beam with $w = 10$ mm after collimated and broadened by a telescope system. Meanwhile, the IMI, simulated by the intensity-only SLM (SLM_2, Holoeye LC-R 1080), is placed in front of the Fourier lens with the focal length of $f = 1000$ mm. We placed Fresnel lens L_1 in an $f - f$ geometry system, imaging the far-field diffraction pattern of the plate. The far-field diffraction intensity pattern was recorded by a digital camera with the pixel size of 3.45 μm. We used SLMs to generate vortex beams (SLM_1) and to create the desired IMI (SLM_2), respectively. The polarization state of the beam produced by the helium-neon laser is controlled by the polarizer, collimated and expanded by the lens, and sent to the phase-only

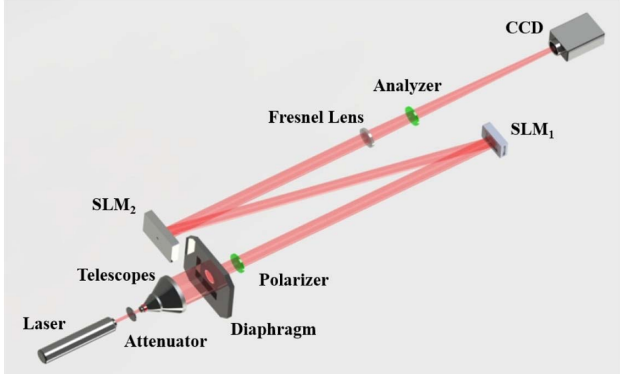

Fig. 4. Schematic overview of the setup for measuring OAM of the vortex beams.

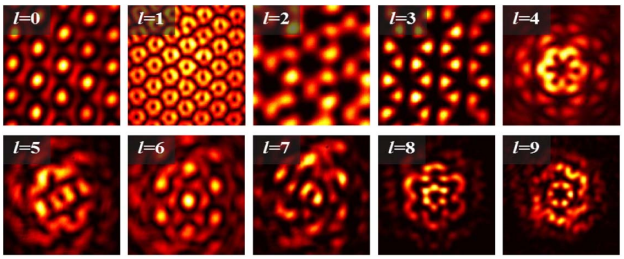

Fig. 5. Experimental results of the far-field intensity patterns corresponding to Fig. 2(a).

SLM_1. A diaphragm allowed selecting the desired diffraction order, which was generated by spiral phase plate displayed on SLM_1. The desired plate created by the SLM_2 is in the front focal plane of the Fourier-transforming lens. By using this $f-f$ optical system, the far-field diffraction patterns of the plate were imaged onto the CCD camera. We used an analyzer to ensure appropriate state incidence on the CCD camera.

The far-field diffraction intensity patterns recorded in our experiment, for different topological charges, are shown in Fig. 5, where it is shown that the experimental results agree well with the simulations shown in Fig. 2. Figure 5 also shows that an IMI with larger apertures enables us to characterize high topological charge from the diffracted intensity patterns.

4. CONCLUSIONS

In conclusion, we demonstrated an approach to measure the OAM of vortex beams by distinguishing the far-field intensity patterns with an IMI. This robust method is as simple as MI; accordingly, it can be used to measure the OAM of light from astronomical sources as well. The only difference between IMI and MI is the size of pinholes. The bigger pinholes in IMI enable us to measure the high topological charge of vortex beams. Furthermore, we want to claim that our method is available for measuring the OAM of Bessel vortex beams as well, and the robust IMI is also applicable to other scalar vortex waves with larger topological charge, such as electron vortex beams, neutron vortex beams, and X-ray vortex beams. The IMI will be useful for many applications based on OAM [6,7,36].

Funding. National Natural Science Foundation of China (11874102); Sichuan Province Science and Technology Support Program (20CXRC0086); Fundamental Research Funds for the Central Universities (ZYGX2019J102).

Disclosures. The authors declare no conflicts of interest.

REFERENCES

1. M. Yao and M. J. Padgett, "Orbital angular momentum: origins, behavior and applications," Adv. Opt. Photon. **3**, 161–204 (2011).
2. L. Allen, M. W. Beijersbergen, R. J. C. Spreeuw, and J. P. Woerdman, "Orbital angular momentum of light and the transformation of Laguerre-Gaussian laser modes," Phys. Rev. A **45**, 8185 (1992).
3. F. Ricci, W. Löffler, and M. P. van Exter, "Instability of higher-order optical vortices analyzed with a multi-pinhole interferometer," Opt. Express **20**, 22961–22975 (2012).
4. A. Mair, A. Vaziri, G. Weihs, and A. Zeilinger, "Entanglement of the orbital angular momentum states of photons," Nature **412**, 313–316 (2001).
5. A. Vaziri, J. Pan, T. Jennewein, G. Weihs, and A. Zeilinger, "Concentration of higher dimensional entanglement: qutrits of photon orbital angular momentum," Phys. Rev. Lett. **91**, 227902 (2003).
6. J. Wang, "Advances in communications using optical vortices," Photon. Res. **4**, B14–B28 (2016).
7. J. Leach, J. Courtial, and S. M. Barnett, "Interferometric methods to measure orbital and spin, or the total angular momentum of a single photon," Phys. Rev. Lett. **92**, 013601 (2004).
8. J. Keller, A. Schönle, and S. W. Hell, "Efficient fluorescence inhibition patterns for RESOLFT microscopy," Opt. Express **15**, 3361–3371 (2007).
9. K. Ladavac and D. G. Grier, "Microoptomechanical pumps assembled and driven by holographic optical vortex arrays," Opt. Express **12**, 1144–1149 (2004).
10. Y. Shen, Z. Wan, Y. Meng, X. Fu, and M. Gong, "Polygonal vortex beams," IEEE Photon. J. **10**, 1503016 (2018).
11. M. Harwit, "Photon orbital angular momentum in astrophysics," Astrophys. J. **597**, 1266–1270 (2003).
12. Y. Yang, M. Mazilu, and K. Dholakia, "Measuring the orbital angular momentum of partially coherent optical vortices through singularities in their cross-spectral density functions," Opt. Lett. **37**, 4949–4951 (2012).
13. S. Zheng, Y. Li, Q. Lin, X. Zeng, G. Zheng, Y. Cai, Z. Chen, S. Xu, and D. Fan, "Experimental realization to efficiently sort vector beams by polarization topological charge via Pancharatnam-Berry phase modulation," Photon. Res. **6**, 385–389 (2018).
14. Y. Yang and Y. Liu, "Measuring azimuthal and radial mode indices of a partially coherent vortex field," J. Opt. **18**, 015604 (2016).
15. H. Ma, X. Li, Y. Tai, H. Li, J. Wang, M. Tang, Y. Wang, J. Tang, and Z. Nie, "*In situ* measurement of the topological charge of a perfect vortex using the phase shift method," Opt. Lett. **42**, 135–138 (2017).
16. Y. Shen, X. Wang, Z. Xie, C. Min, X. Fu, Q. Liu, M. Gong, and X. Yuan, "Optical vortices 30 years on: OAM manipulation from topological charge to multiple singularities," Light: Sci. Appl. **8**, 90 (2019).
17. G. Gibson, J. Courtial, M. J. Padgett, M. Vasnetsov, V. Pas'ko, S. M. Barnett, and S. Franke-Arnold, "Free-space information transfer using light beams carrying orbital angular momentum," Opt. Express **12**, 5448–5456 (2004).
18. J. Leach, M. Padgett, S. Barnett, S. Franke-Arnold, and J. Courtial, "Measuring the orbital angular momentum of a single photon," Phys. Rev. Lett. **88**, 257901 (2002).
19. H. I. Sztul and R. R. Alfano, "The Poynting vector and angular momentum of Airy beams," Opt. Express **16**, 9411–9416 (2018).
20. G. C. G. Berkhout and M. W. Beijersbergen, "Method for probing the orbital angular momentum of optical vortices in electromagnetic waves from astronomical objects," Phys. Rev. Lett. **101**, 100801 (2008).
21. C. Guo, S. Yue, and G. Wei, "Measuring the orbital angular momentum of optical vortices using a multipinhole plate," Appl. Phys. Lett. **94**, 231104 (2009).
22. G. C. G. Berkhout, M. P. J. Lavery, J. Courtial, M. W. Beijersbergen, and M. J. Padgett, "Efficient sorting of orbital angular momentum states of light," Phys. Rev. Lett. **105**, 153601 (2010).
23. H. Zhou, L. Shi, X. Zhang, and J. Dong, "Dynamic interferometry measurement of orbital angular momentum of light," Opt. Lett. **39**, 6058–6061 (2014).
24. D. Fu, D. Chen, R. Liu, Y. Wang, H. Gao, F. Li, and P. Zhang, "Probing the topological charge of a vortex beam with dynamic angular double slits," Opt. Lett. **40**, 788–791 (2015).
25. S. Fu, T. Wang, Y. Gao, and C. Gao, "Diagnostics of the topological charge of optical vortex by a phase-diffractive element," Chin. Opt. Lett. **14**, 080501 (2016).
26. J. Narag and N. Hermosa, "Probing higher orbital angular momentum of Laguerre-Gaussian beams via diffraction through a translated single slit," Phy. Rev. Appl. **11**, 054025 (2019).
27. S. N. Alperin, R. D. Niederriter, J. T. Gopinath, and M. E. Siemens, "Quantitative measurement of the orbital angular momentum of light with a single, stationary lens," Opt. Lett. **41**, 5019–5022 (2016).

28. S. Fu, S. Zhang, T. Wang, and C. Gao, "Measurement of orbital angular momentum spectra of multiplexing optical vortices," Opt. Express **24**, 6240–6248 (2016).
29. J. Zhu, P. Zhang, D. Fu, D. Chen, R. Liu, Y. Zhou, H. Gao, and F. Li, "Probing the fractional topological charge of a vortex light beam by using dynamic angular double slits," Photon. Res. **4**, 187–190 (2016).
30. D. Deng, M. Lin, Y. Li, and H. Zhao, "Precision measurement of fractional orbital angular momentum," Phy. Rev. Appl. **12**, 014048 (2019).
31. Y. Shen, X. Fu, and M. Gong, "Truncated triangular diffraction lattices and orbital-angular-momentum detection of vortex SU(2) geometric modes," Opt. Express **26**, 25545–25557 (2018).
32. Y. Yang, Q. Zhao, L. Liu, Y. Liu, C. Rosales-Guzmán, and C.-W. Qiu, "Manipulation of orbital-angular-momentum spectrum using pinhole plates," Phys. Rev. Appl. **12**, 064007 (2019).
33. L. Shi, L. Tian, and X. Chen, "Characterizing topological charge of optical vortex using non-uniformly distributed multi-pinhole plate," Chin. Opt. Lett. **10**, 120501 (2012).
34. J. Arlt, K. Dholakia, L. Allen, and M. J. Padgett, "Parametric down-conversion for light beams possessing orbital angular momentum," Phys. Rev. A **59**, 3950–3952 (1999).
35. H. Ma, X. Li, H. Zhang, J. Tang, H. Li, M. Tang, J. Wang, and Y. Cai, "Optical vortex shaping via a phase jump factor," Opt. Lett. **44**, 1379–1382 (2019).
36. D. Cozzolino, E. Polino, M. Valeri, G. Carvacho, D. Bacco, N. Spagnolo, L. K. Oxenløwe, and F. Sciarrinob, "Air-core fiber distribution of hybrid vector vortex-polarization entangled states," Adv. Photon. **1**, 046005 (2019).